

## Development of subaqueous barchanoid-shaped dunes due to lateral grain size variability in a tidal inlet channel of the Danish Wadden Sea

Verner B. Ernstsen, Riko Noormets, Christian Winter, and Dierk Hebbeln  
 Research Center Ocean Margins, University of Bremen, Bremen, Germany

Alex Bartholomä and Burg W. Flemming  
 Division of Marine Science, Senckenberg Institute, Wilhelmshaven, Germany

Jesper Bartholdy  
 Institute of Geography, University of Copenhagen, Copenhagen, Denmark

Received 11 June 2004; revised 6 January 2005; accepted 27 January 2005; published 4 October 2005.

[1] High-resolution bathymetry at centimeter-scale accuracy acquired with a multibeam echo sounder system revealed the existence of barchanoid-shaped large (i.e., length 10–100 m) to very large (i.e., length >100 m) dunes in the Grådyb tidal inlet channel in the Danish Wadden Sea. The development of these dunes is due to an increase in dune celerity from 12 m/yr in the center of the channel to around 30 m/yr at the sides. This increase in dune celerity can be explained by the fact that dune heights decrease from 3.1 m in the center of the channel to 1.4 m at the sides, as a smaller sediment volume has to be moved per unit time for equal dune celerity. Water depth is uniform across the channel. Likewise, high-resolution acoustic Doppler current profiler measurements across the channel showed a uniform distribution of both ebb and flood flow. Thus no correlation between dune dimensions and water depth or flow velocity was established. Instead, high-accuracy bed sampling along the crests of the dunes showed a decrease in mean grain size from 0.63 mm in the center to 0.36 mm at the sides of the channel. The decrease in dune height is ascribed to this decrease in grain size, given that flow depth and flow velocity are uniform across the channel. The lateral decrease in grain size is suggested to result from sorting effects by secondary currents directed from the center toward the sides of the channel in the trough/lee side region of the barchanoid-shaped dunes.

**Citation:** Ernstsen, V. B., R. Noormets, C. Winter, D. Hebbeln, A. Bartholomä, B. W. Flemming, and J. Bartholdy (2005), Development of subaqueous barchanoid-shaped dunes due to lateral grain size variability in a tidal inlet channel of the Danish Wadden Sea, *J. Geophys. Res.*, 110, F04S08, doi:10.1029/2004JF000180.

### 1. Introduction

[2] Tidal inlets are narrow natural channels that connect the open sea with a lagoon, as is often the case in barrier-island systems. The channel beds are typically covered with bed forms [Flemming and Davis, 1992; Hennings *et al.*, 2004], the dimensions of which are controlled by the local hydrodynamics and sediment characteristics [Allen, 1982; Flemming, 2000a, 2000b]. Because of the generally narrow shape of tidal inlets, the flow velocities are often high (>1 m/s) and bed material is accordingly composed of sandy material [Flemming and Davis, 1992]. To understand the dynamics of bed forms, numerous studies have been conducted in rivers [e.g., Sukhodolov *et al.*, 1998; Carling *et al.*, 2000], in tidal environments [e.g., Dalrymple *et al.*, 1978; Harbor, 1998] and on the continental shelf [e.g.,

Flemming, 1978; Arduin *et al.*, 2002]. However, earlier studies have primarily been based on single longitudinal profiles [e.g., Van den Berg, 1987; Bartholdy *et al.*, 2002], which have revealed rather little about the lateral shape of dunes. A few exceptions include the Fraser River, Canada, where Kostaschuk and Villard [1996] observed dunes with a curved, concave downstream planform with 300 m long crest lines. Carling *et al.* [2000] observed barchan dunes in the River Rhine, Germany, extending approximately 120 m across the channel. Recently, Dinehart [2002] described dunes in the San Joaquin River, United States, with crests oriented about 45° from the banks. Barchanoid-shaped dunes can also be identified on the bathymetric data presented by Abraham and Pratt [2002] from the Upper Mississippi River, United States. Nevertheless, these detailed field studies still focus on the longitudinal dune patterns and not on the lateral shapes of the dunes. Only one recent flume study has described the lateral flow distribution over sinuous-crested three-dimensional dunes

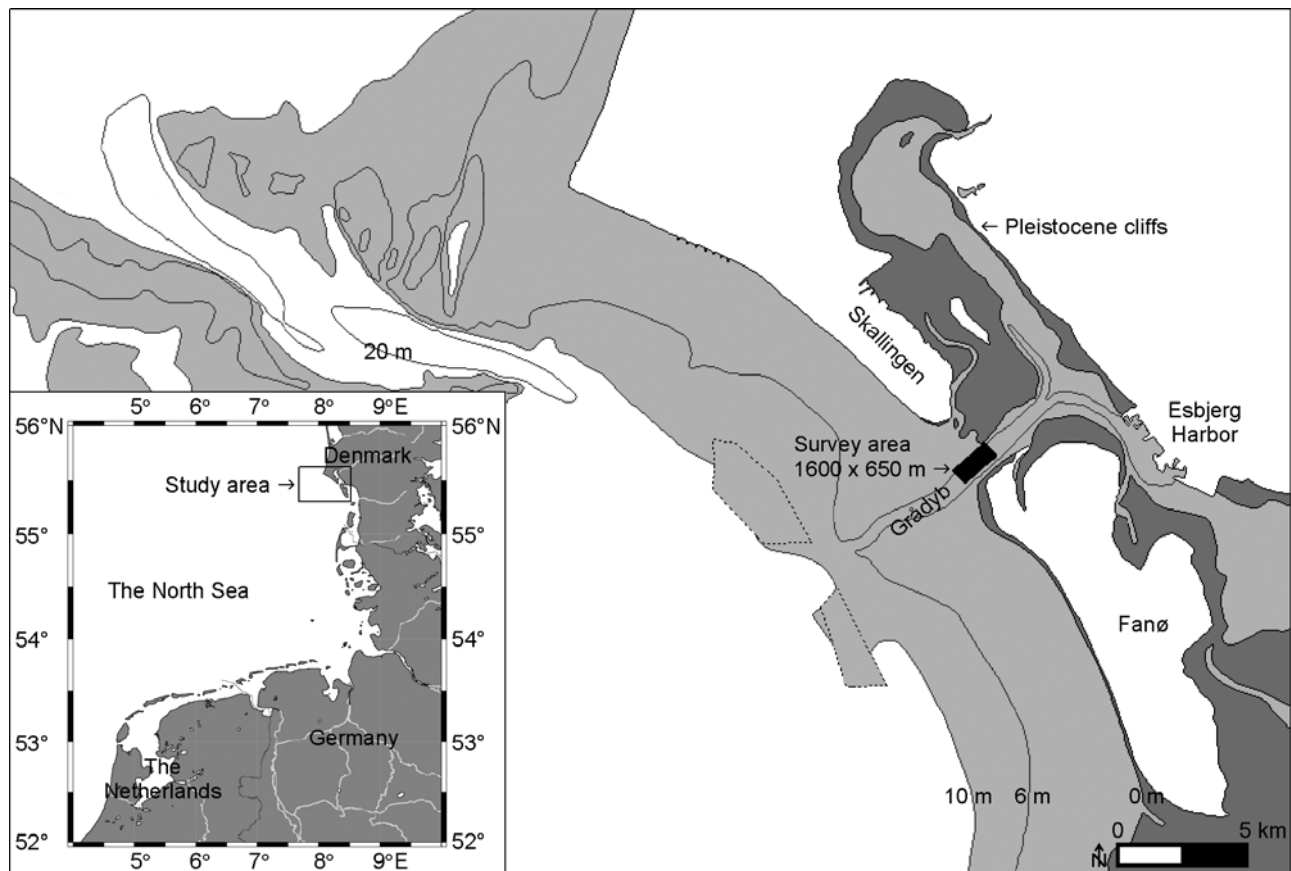


**Figure 1.** Location of the study area in the Grådyb tidal inlet channel between the barrier spit of Skallingen and the barrier island of Fanø in Denmark. Water depths are relative to mean low water springs (MLWS). The two zones encircled by dashed lines are dumping sites for dredged material.

[Maddux *et al.*, 2003a, 2003b]. To the knowledge of the authors, no studies have dealt with lateral grain size patterns over dunes.

[3] This study investigates the potential influence of lateral, i.e., cross-channel, variations in water depth, flow velocity and grain size patterns on the development of subaqueous barchanoid-shaped dunes in the Grådyb tidal inlet channel in the Danish Wadden Sea (Figure 1). The term barchanoid is solely used to describe the lateral shape of the dunes and the net direction of migration since the flow is not unidirectional but bidirectional. In addition, there is an abundance of sediment, no lack; and the dunes are thus not migrating over firm ground.

## 2. Study Area

[4] The Grådyb tidal inlet is located on the Danish west coast between the barrier spit of Skallingen to the northwest and the barrier island of Fanø to the southeast. It connects the northernmost tidal basin of the Wadden Sea with the adjacent North Sea (Figure 1).

[5] The tides are semidiurnal with a mean tidal range of about 1.5 m and a tidal prism in the order of  $150 \times 10^6 \text{ m}^3$  [Bartholdy and Anthony, 1998]. The width of the channel is roughly 1 km and the mean depth is 10–13 m. The channel is ebb-dominated with maximum ebb and flood current velocities around 1.50 m/s and 1.25 m/s, respectively

[Bartholdy and Anthony, 1998]. The bed of the channel is composed of sand with mean grain sizes ranging from 0.3 to 0.7 mm. There are two sediment sources in the area; one being the Pleistocene cliffs lining the mainland in the landward part of the back-barrier tidal basin (Figure 1), it supplies medium to coarse sand. The other, which supplies fine sand to the tidal inlet, is located in the nearshore region of the open coast [Bartholdy *et al.*, 2002].

## 3. Methods

### 3.1. Surveys and Instruments

[6] Bathymetric surveys were conducted in a  $1600 \times 650 \text{ m}$  section of the channel (for location, see Figure 1) on 10 September 2002 and 11 July 2003. The bathymetric data were recorded using a Seabat 8125™ (RESON) multibeam echo sounder (MBES) system operating at 455 kHz and the 6042 v. 7™ (RESON/QPS) data collecting and processing software package. The vertical resolution of the MBES system is in a subcentimeter scale (<http://www.reson.com>). The lateral resolution is a function of water depth and vessel speed. For instance, a water depth of 15 m results in an across-track resolution of 0.13–0.52 m due to the across-track beam width of  $0.5^\circ$ ; at a vessel speed of 2.6 m/s (5 kn) the along-track resolution is 0.10 m. Therefore a cell size of  $0.5 \times 0.5 \text{ m}$  was chosen for the gridding of the bathymetric data. The MBES system was coupled with an AQUARIUS

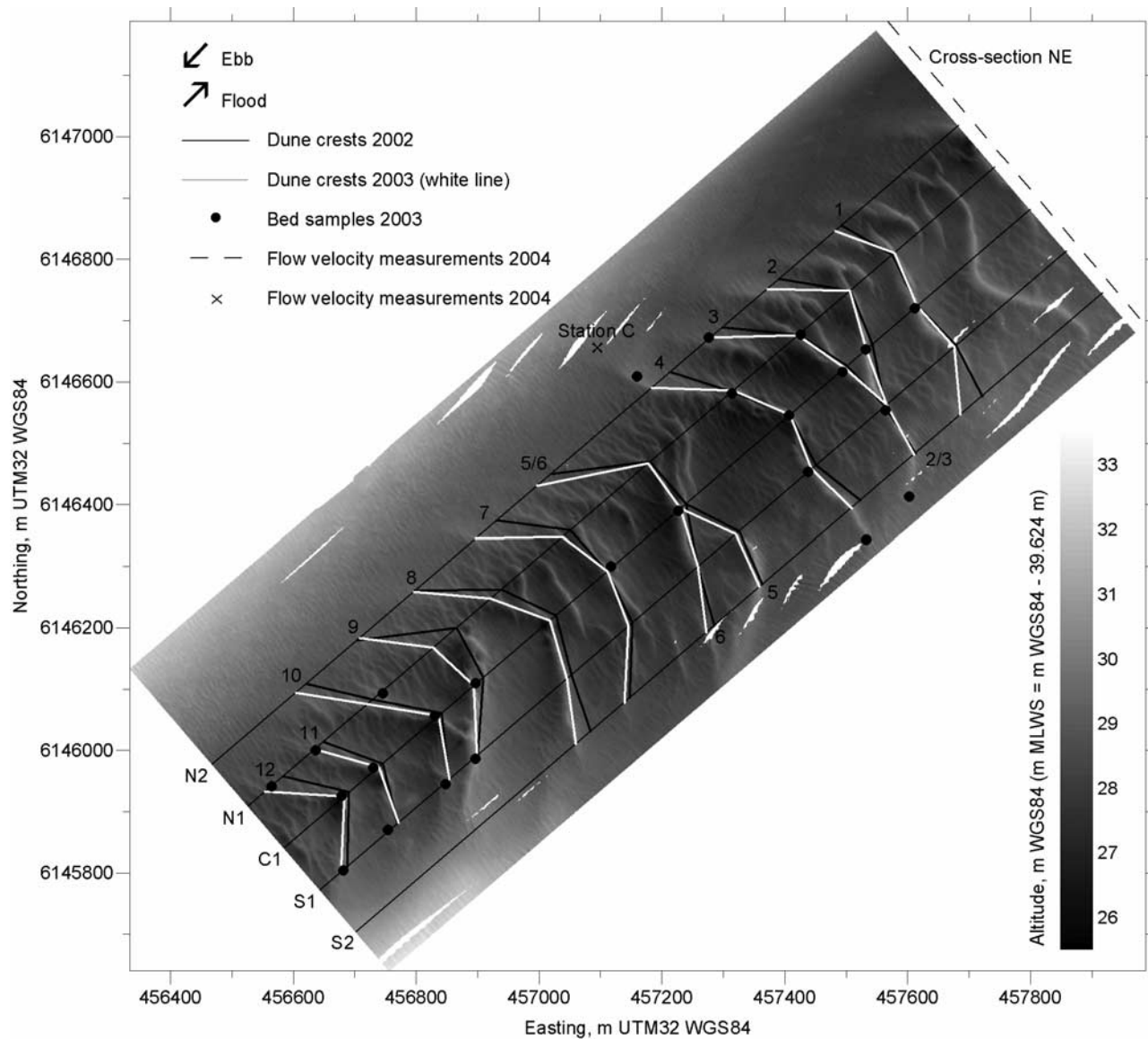


**Figure 2.** Bathymetry of the Grådyb tidal inlet channel in 2003. The grid is  $1600 \times 650$  m with a cell size of  $0.5 \times 0.5$  m. Dune crests extending across the channel in both 2002 and 2003 are marked with black and white lines, respectively, and numbered from 1 to 12. Bed profiles were extracted along transects N2-S2 (see Figure 3). Bed samples (marked with dots) were collected from dune crests along transects N2-S2 in 2003 (see Figures 6 and 7). ADCP measurements were conducted along cross section NE over 10 hours of a tidal period at spring tide in 2004 (see Figures 4 and 5). Water depth relative to mean low water springs (MLWS) in relation to WGS84 altitude is given by  $m \text{ MLWS} = m \text{ WGS84} - 39.624 \text{ m}$ .

5002™ (THALES/DSNP) dual frequency (L1/L2) Long Range Kinematic (LRK™) Global Positioning System (GPS). The vertical and lateral accuracy of the positioning system is better than 0.05 m [Lutz and Gounon, 2001]. Altitudes are presented in relation to UTM32 WGS84 map projections. Corrections for ship movements were applied using an Octans Surface™ (IXSEA OCEANO) gyrocompass and motion sensor.

[7] Flow velocities were measured along cross section NE over 10 hours of a tidal period, as well as at station C over a whole tidal period around spring tide on 3 July 2004 (for locations, see Figure 2). Along cross section NE the flow velocity data were collected using a Workhorse Sentinel™

(RDI) acoustic Doppler current profiler (ADCP) operating at 1200 kHz and the WinRiver™ (RDI) software package. The vertical resolution of the ADCP was set to 0.25 m and the lateral resolution is approximately 5 m at a ping rate of 2 Hz and a vessel speed of 2.6 m/s (5 kn). At station C, the flow velocity data were collected using a Niskin 6011 MKII winged current meter attached to a submerged mooring system. The current meter was located approximately 4 m above the bed at a water depth varying between 10 and 12 m. Flow velocity values were recorded every 5 min, being averaged over 40 discrete measurements in each case.

[8] Bed material was collected from bed form crests along the five transects N2-S2 (for locations, see Figure 2)

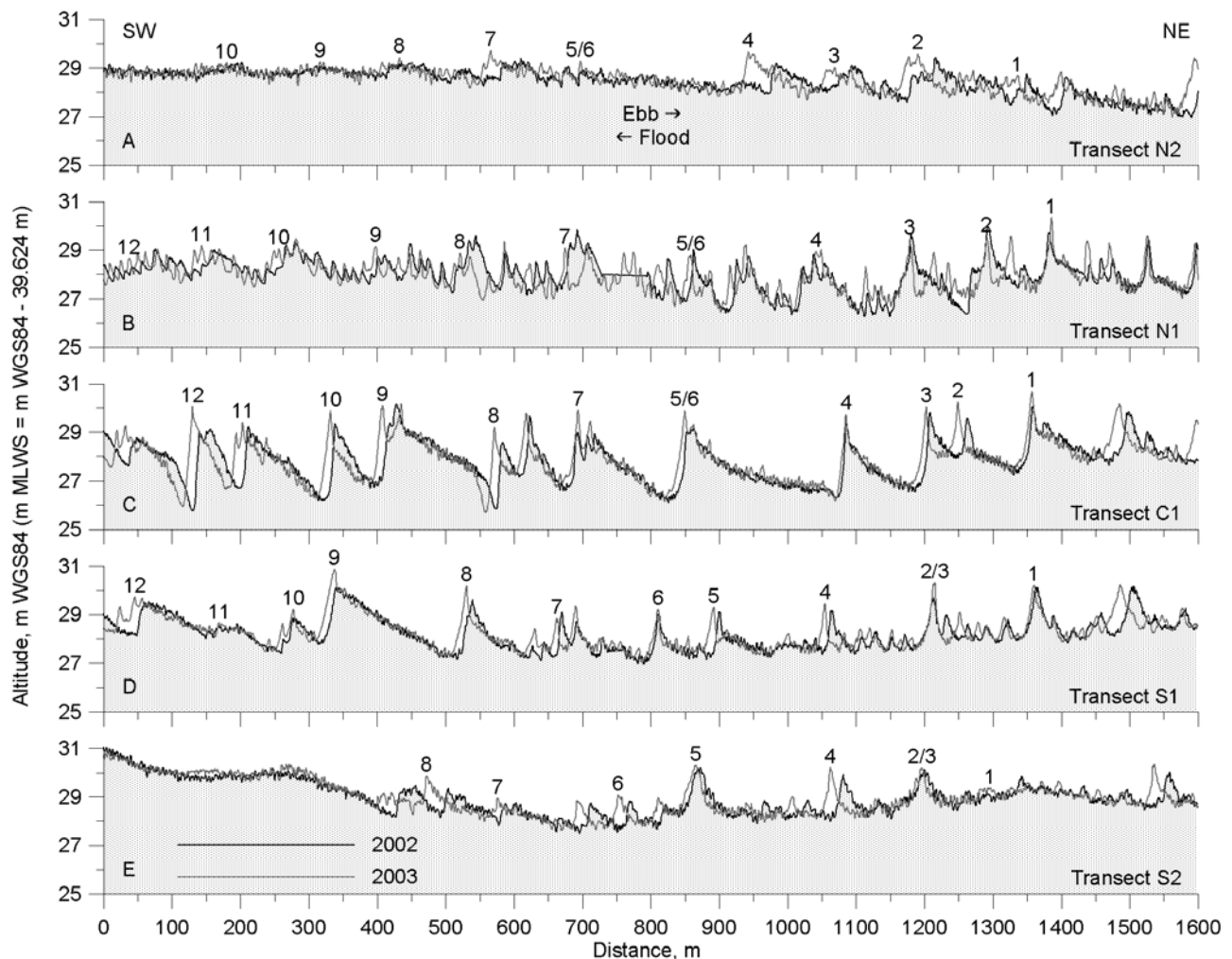


**Figure 3.** Bed profiles along transects N2-S2 (A–E) extracted from bathymetric grids with cell sizes of  $0.5 \times 0.5$  m from 2002 and 2003 (for locations, see Figure 2). Dune dimensions and celerities were determined from the identified (numbered from 1 to 12) large to very large dunes.

on 14 July 2003 using a Shipek™ grab sampler. Sampling positions were determined by the high-accuracy positioning system described above. The drift of the grab sampler during lowering through the water column determines the inaccuracy in the sampling positioning, which was assessed to be better than 2 m based on the water depths and the observed cable angles.

### 3.2. Bed Form Dimensions and Celerities

[9] Bed form dimensions and celerities were determined from the gridded bathymetry in 2002 and 2003 along the five transects N2-S2. Only bed forms with crests extending across the entire channel in both 2002 and 2003 were considered. Bed form length  $L$  has been defined as the trough-to-trough distance with the location of a trough defined as the lowest point of the lee (or stoss) side of a bed form. Bed form height  $H$  was determined as the vertical distance from the crest to the line defining the bed form length. The location of the crest was defined as the highest point along the bed form. However, there were a few exceptions (see Figures 2 and 3) where the determined crests differed from the highest points, but instead displayed

a secondary maximum along the bed forms. These departures were due to the fact that the crests extending across the entire channel in both 2002 and 2003, in a few cases, deviated from the highest points along the bed forms in one of the two years. The effect on the calculated bed form heights, though, was insignificant, as the deviations were small compared to the heights of the bed forms. Bed form volume per unit width  $V$  was calculated by integrating over the area above the line defining the bed form length. The bed form shape factor  $\beta$  was then calculated by relating the bed form volume per unit width to the product of bed form length and height ( $\beta = V/LH$ ). Bed form celerity  $c$  was calculated for each bed form as the average movement of the troughs and the crest from 2002 to 2003. The bed form celerities are presented in meters per year although the calculations are based on two surveys only 10 months apart. The bed forms have been described according to the classification recommended by Ashley [1990], where ripples ( $L < 0.6$  m) and dunes ( $L > 0.6$  m) are distinguished on the basis of bed form length, dunes being further divided into categories of small ( $L = 0.6$ –5 m), medium ( $L = 5$ –10 m), large ( $L = 10$ –100 m) and very large ( $L > 100$  m).

### 3.3. Water Depths and Flow Velocities

[10] The average water depth  $D$  relative to mean low water springs (MLWS) was also determined along transects N2-S2 based on the bathymetric grids from 2002 and 2003. Furthermore, average water depths were calculated in discrete time steps over a tidal period along the part of cross section NE bounded by transects N2 and S2 (for location, see Figure 2) likewise based on the bathymetric grids from 2002 and 2003. Subsequently, the average cross-section water depths were used in the predictions of bed load transport.

[11] Flow velocities were measured along cross section NE at approximately half-hourly intervals. In each case, the profile was run twice (10–15 min in total) with the repetition serving as a quality control of the data, besides increasing the lateral resolution of data points. At each measuring point along the cross section, the mean flow velocity (depth averaged)  $U$  was determined as the ensemble average flow velocity. These point mean flow velocities were then used to calculate the average mean flow velocity in the part of cross section NE bounded by transects N2 and S2. Relating these average cross-section mean flow velocities to the flow velocities measured at station C revealed a significant linear correlation with the regression line  $U_{NE} = 1.03u_C$  ( $r = 0.992$ ,  $n = 20$ ,  $p < 0.0005$ ). This regression was used to extrapolate the 10-hour measurements along cross section NE to cover the entire tidal period. Subsequently, the cross-section mean flow velocities were used in the predictions of bed load transport.

### 3.4. Grain Size Analysis

[12] After rinsing the samples to remove salt and washing through a 4 phi (0.063 mm) wet sieve to separate sand and silt/clay, the samples were dried in the oven at 70°C and sieved at 1/4 phi intervals. Where present, the mud fractions were collected, dried, and weighed to be subsequently added to the size distributions without being further analyzed.

[13] Mean grain size  $d_{MZ}$ , phi standard deviation  $\sigma_I$ , phi skewness  $Sk_I$  and phi kurtosis  $K_G$  of the grain size distributions were determined on the basis of the percentile statistics described by *Folk and Ward* [1957].

### 3.5. Bed Load Transport Based on Measured Bathymetry

[14] Volumetric bed load transport  $q_b$  was too calculated along transects N2-S2 from the measured bathymetry, as well as from classical and widely applied bed load transport formulae.

[15] Knowing bed form migration in conjunction with bed form dimensions, the volumetric bed load transport can be quantified according to the equation originally suggested by *Simons et al.* [1965]:

$$q_b = \beta cH \quad (1)$$

where  $\beta$  is the shape factor,  $c$  is bed form celerity and  $H$  is bed form height. The shape factor is equal to 0.5 in case of idealized triangular bed forms [e.g., *Simons et al.*, 1965; *Engel and Lau*, 1980]. However, in nature the shape factor often deviates from 0.5 and quite a few authors have found a value around 0.6 to be more appropriate [*Van den Berg*,

1987; *Kostaschuk et al.*, 1989; *Villard and Church*, 2003]. The applicability of equation (1) to quantify bed load transport has been discussed repeatedly in earlier studies [e.g., *Engel and Lau*, 1980, 1981; *Van den Berg*, 1987; *Wilbers and Ten Brinke*, 2003; *Hoekstra et al.*, 2004]. The most recent review by *Hoekstra et al.* [2004] concludes that equation (1) is adequate to determine bed load transport. Consequently, this approach was applied in this study, i.e., simply calculating bed load transport by inserting the appropriate values in equation (1). Furthermore, as also recommended by *Hoekstra et al.* [2004], bed form-specific shape factors were used instead of a constant shape factor.

### 3.6. Prediction of Bed Load Transport

[16] When bed forms are present, the bed shear stress can be divided into a grain-related bed shear stress due to skin friction and a form-related bed shear stress due to form friction [e.g., *Fredsøe and Deigaard*, 1992]. The grain-related bed shear stress is the effective shear stress acting on the bed, whereas the form-related bed shear stress originates from the normal stress associated with the fluid pressure distribution upstream and downstream of the bed form crest [*Van Rijn*, 1993]. Since sediment is moved by the effective shear stress and is unaffected by the normal stress, only the skin friction component of the total bed shear stress should be used [*Soulsby*, 1997]. Four bed load transport formulae were applied to calculate volumetric bed load transport: the classical *Meyer-Peter and Müller* [1948] formula and the widely applied formulae of *Engelund and Fredsøe* [1976], *Van Rijn* [1984a], and *Nielsen* [1992] developed during the last three decades. According to these formulae, the dimensionless bed load transports  $\Phi_b$  are given by

*Meyer-Peter and Müller* [1948]

$$\Phi_b = 8(\theta' - \theta_{cr})^{1.5} \quad (2)$$

*Engelund and Fredsøe* [1976]

$$\Phi_b = \frac{5}{\left[1 + \frac{0.005}{(\theta' - \theta_{cr})^4}\right]^{0.25}} \left(\sqrt{\theta'} - 0.7\sqrt{\theta_{cr}}\right) \quad (3)$$

*Van Rijn* [1984a]

$$\Phi_b = 0.053 \frac{T^{2.1}}{D_*^{0.3}}, \quad T < 3 \quad (4a)$$

$$\Phi_b = 0.1 \frac{T^{1.5}}{D_*^{0.3}}, \quad T \geq 3 \quad (4b)$$

*Nielsen* [1992]

$$\Phi_b = 12\sqrt{\theta'}(\theta' - \theta_{cr}) \quad (5)$$

where  $\theta'$  is the grain-related Shield's parameter,  $\theta_{cr}$  is the threshold Shield's parameter,  $T = (\theta' - \theta_{cr})/\theta_{cr}$  is the excess bed shear stress parameter and  $D_*$  is the particle parameter. The latter is defined as

$$D_* = \left[\frac{(s-1)g}{\nu^2}\right]^{\frac{1}{3}} d_{50} \quad (6)$$

in which  $s = \rho_s/\rho$  is the relative sediment density,  $\rho_s$  is the sediment density corresponding to that of quartz particles ( $2650 \text{ kg/m}^3$ ),  $\rho$  is the density of water ( $1022 \text{ kg/m}^3$  at a temperature of  $17^\circ\text{C}$  and a salinity of 31 ppt as measured on 3 July 2004),  $g$  is the acceleration due to gravity ( $9.81 \text{ m/s}^2$ ),  $\nu$  is the kinematic viscosity ( $1.08 \times 10^{-6} \text{ m}^2/\text{s}$  at the temperature and salinity mentioned above) and  $d_{50}$  is median grain size. The threshold Shield's parameter is calculated by the formula suggested by *Soulsby and Whitehouse* [1997]:

$$\theta_{cr} = \frac{0.30}{1 + 1.2D_*} + 0.055 \left[ 1 - \exp(-0.020D_*) \right] \quad (7)$$

The grain-related Shield's parameter is calculated by

$$\theta' = \frac{u_f'^2}{(s-1)g d_{50}} \quad (8)$$

where  $u_f'$  is the friction velocity. For turbulent flow the friction velocity can be calculated from the Chézy equation:

$$u_f' = \sqrt{g} \frac{U}{C'} \quad (9)$$

where  $U$  is mean flow velocity (depth averaged) and  $C'$  is the grain related Chézy roughness coefficient which for rough flow is given by

$$C' = 18 \log \left( \frac{12D}{k'_s} \right) \quad (10)$$

in which  $D$  is water depth and  $k'_s$  is the grain roughness. *Meyer-Peter and Müller* [1948] and *Van Rijn* [1984a] relate the grain roughness to the coarse 90th percentile of the grain size distribution  $d_{90}$ , i.e., for *Meyer-Peter and Müller* [1948],  $k'_s = d_{90}$ , whereas for *Van Rijn* [1984a],  $k'_s = 3d_{90}$ . By contrast, *Engelund and Fredsøe* [1976] and *Nielsen* [1992] relate the grain roughness to the median grain size  $d_{50}$ , i.e.,  $k'_s = 2.5d_{50}$ . Finally, dimensionless bed load transport is transformed to volumetric bed load transport according to

$$\Phi = \frac{q_b}{\sqrt{(s-1)g d_{50}^3}} \quad (11)$$

[17] Just as the magnitude of the flow varies during a tidal period, the direction of the flow also changes with ebb and flood. For that reason, flow velocities are considered positive during flood and negative during ebb. Consequently, bed load transport is also positive during flood while negative during ebb.

## 4. Observations

### 4.1. Observed Dune Dimensions and Celerities

[18] The bed of the Grådyb tidal inlet channel is covered with large to very large compound dunes (Figure 2). In total, 12 dunes extending across the channel in both 2002 and 2003 were identified along transects N2-S2 (Figure 2). Following the dune crests across the channel, the dunes display barchanoid shapes (Figure 2).

**Table 1.** Average Dune Length  $L$ , Height  $H$ , Volume per Unit Width  $V$ , Shape Factor  $\beta$ , Celerity  $c$ , Water Depth  $D$ , Mean Grain Size  $d_{MZ}$ , Coarse 90th Percentile of the Grain Size Distribution  $d_{90}$ , Phi Standard Deviation  $\sigma_I$ , Phi Skewness  $Sk_I$ , and Phi Kurtosis  $K_G$  Along Transects N2-S2<sup>a</sup>

	N2	N1	C1	S1	S2
$L$ , m	149	137	122	131	152
$H$ , m	1.17	2.21	3.06	1.93	1.57
$V$ , $\text{m}^2$	75	112	147	81	80
$\beta$	0.46	0.38	0.38	0.33	0.36
$c$ , m/yr	31	12	12	9	28
$D$ , m MLWS	11.14	11.67	11.76	11.38	10.63
$d_{MZ}$ , mm	0.357	0.441	0.629	0.460	0.362
$d_{90}$ , mm	0.761	0.777	1.046	0.822	0.634
$\sigma_I$	0.678	0.502	0.499	0.531	0.537
$Sk_I$	-0.279	-0.097	-0.118	-0.121	-0.195
$K_G$	1.379	1.111	1.140	1.103	1.122

<sup>a</sup>For locations, see Figure 2.

[19] Bed profiles along transects N2-S2 extracted from the bathymetric grids from 2002 and 2003 are shown in Figure 3. Dune dimensions and celerities have been calculated from these bed profiles.

[20] The average dune height decreases from 3.06 m in the center of the channel to 1.17 m and 1.57 m at the northern and southern side of the channel, respectively (Table 1). The average dune length, by contrast, increases from 122 m in the center of the channel to 149 m and 152 m at the northern and southern side, respectively (Table 1). The corresponding average dune volume per unit width is  $147 \text{ m}^2$  in the center of the channel, whereas at the northern and southern side it is  $75 \text{ m}^2$  and  $80 \text{ m}^2$ , respectively (Table 1). The average shape factors are relatively constant across the channel, ranging from 0.33 to 0.46 and displaying no clear lateral trend (Table 1).

[21] Along the most southwesterly section of transects N2 and S2, large to very large compound dunes are indiscernible (Figures 3a and 3e). The average dune length and height along the most southwesterly 100 m section of transect N2 is 7.88 m and 0.41 m, respectively (Figure 3a). Along the corresponding section of transect S2, the average dune length and height is 5.16 m and 0.22 m, respectively (Figure 3e).

[22] A comparison of the identified dunes based on the bathymetric grids from 2002 and 2003 reveals a net ebb-directed dune migration (Figures 2 and 3). In the center of the channel the average dune celerity is 12 m/yr whereas at the northern and southern side it is 31 m/yr and 28 m/yr, respectively (Table 1).

### 4.2. Observed Water Depths and Flow Velocities

[23] The average water depth varies from 11.76 m MLWS in the center of the channel to 11.14 m MLWS and 10.63 m MLWS at the northern and southern side, respectively (Table 1). Along the part of cross section NE bounded by transects N2 and S2, the average water depth is 11.36 m MLWS with a standard deviation of 0.62 m.

[24] Mean flow velocities (depth averaged) along cross section NE at four representative stages during a tidal period around spring tide are shown in Figure 4 (the exact times of the four measurements relative to the tidal period are marked with dots in Figure 5). Positive values refer to flood flow and negative values to ebb flow. Around maximum

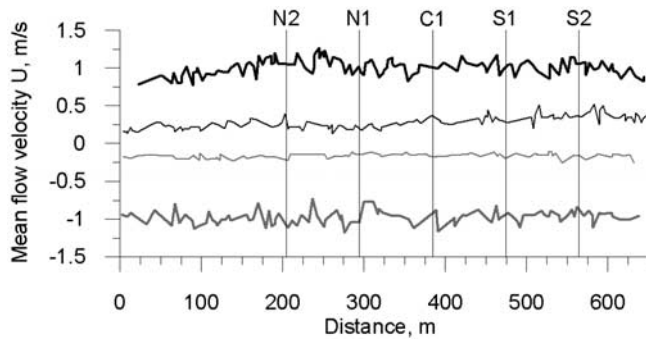


**Figure 4.** Mean flow velocity (depth averaged)  $U$  along cross section NE (for locations, see Figure 2) around spring tide just about maximum flood (thick solid line), close to slack water flood (thin solid line) and ebb (thin shaded line) and the available measurement closest to maximum ebb (thick shaded line). The exact times of the measurements relative to the tidal period are shown with dots in Figure 5.

flood, the cross-section mean flow velocity in the part bounded by transects N2 and S2 is 1.04 m/s with a standard deviation of 0.10 m/s. Close to slack water at the end of the flood phase, the cross-section mean flow velocity is 0.28 m/s with a standard deviation of 0.07 m/s. At the beginning of the ebb phase, the cross-section mean flow velocity is 0.16 m/s with a standard deviation of 0.05 m/s. No measurements are available along cross section NE around maximum ebb flow. However, the measurement closest to maximum ebb displays a cross-section mean flow velocity of 0.97 m/s with a standard deviation of 0.09 m/s. Considering the entire 10-hour measurements during the tidal period, the standard deviations of the cross-section mean flow velocities range from 0.05 m/s to 0.12 m/s with the highest standard deviations around maximum flood and ebb and the lowest close to slack water.

[25] The average mean flow velocities and corresponding average water depths in the part of cross section NE bounded by transects N2 and S2 over a tidal period around spring tide are shown in Figure 5. Cross-section mean flow velocities

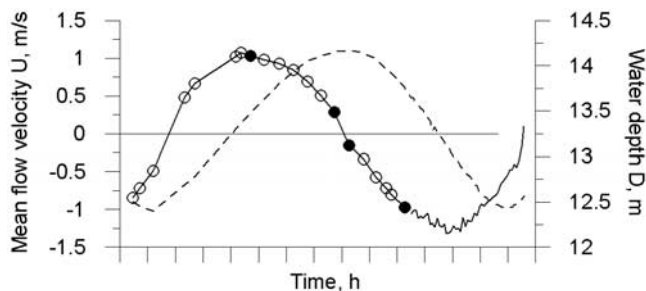


**Figure 5.** Cross-section mean flow velocities  $U$  (solid line) and corresponding average water depths  $D$  (dashed line) in the part of cross section NE bounded by transects N2 and S2 (for location, see Figure 2) over a tidal period around spring tide. Circles and dots mark the times of the ADCP measurements. The extrapolation of the ADCP measurements is determined from the measurements at station C (for location, see Figure 2).

calculated from the cross-section measurements are shown with circles and dots. The extrapolation of the curve is determined from the measurements at station C. The cross-section mean flow velocities during flood and ebb reach maximum values of 1.08 m/s and 1.32 m/s, respectively.

**4.3. Observed Grain Sizes**

[26] Statistics of the bed material collected from dune crests along transects N2-S2 are presented in Figure 6. As examples, the frequency curves of the grain size distributions from the crests of dune 4 and 12 along transects N2-S2 are shown in Figure 7, being representative of grain size distributions across the entire dune field. The average mean

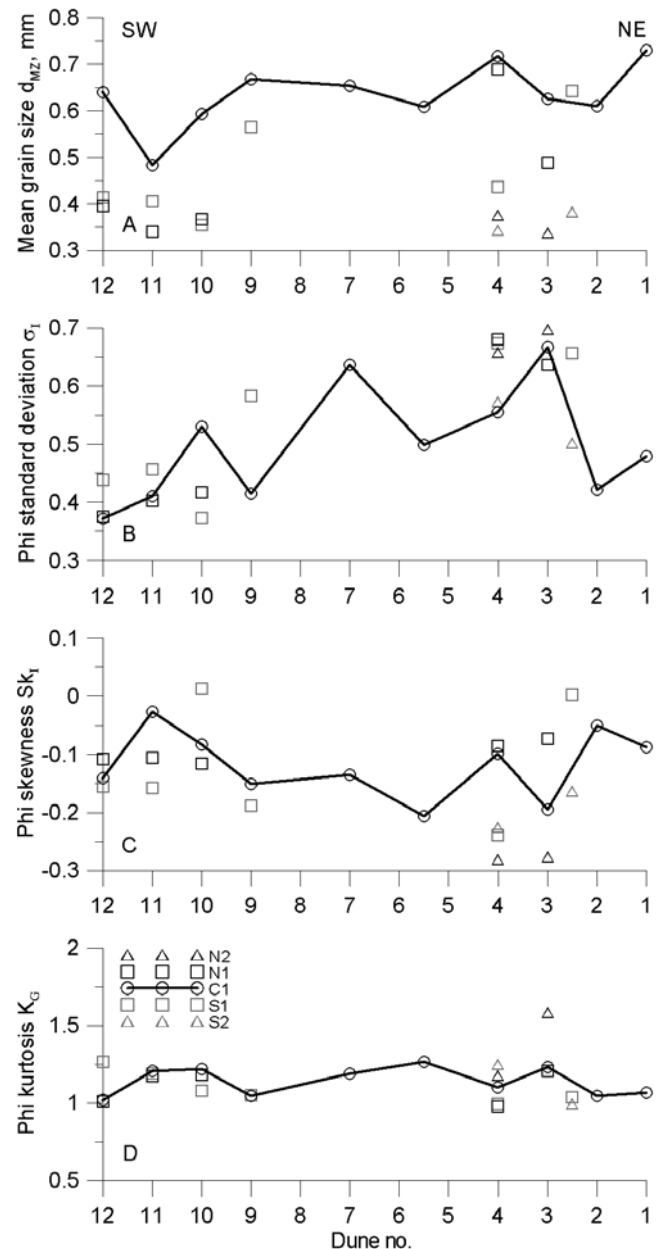


**Figure 6.** (a) Mean grain size  $d_{MZ}$ , (b) phi standard deviation  $\sigma_I$ , (c) phi skewness  $Sk_I$ , and (d) phi kurtosis  $K_G$  at dune crests along transects N2-S2 (for locations, see Figure 2).

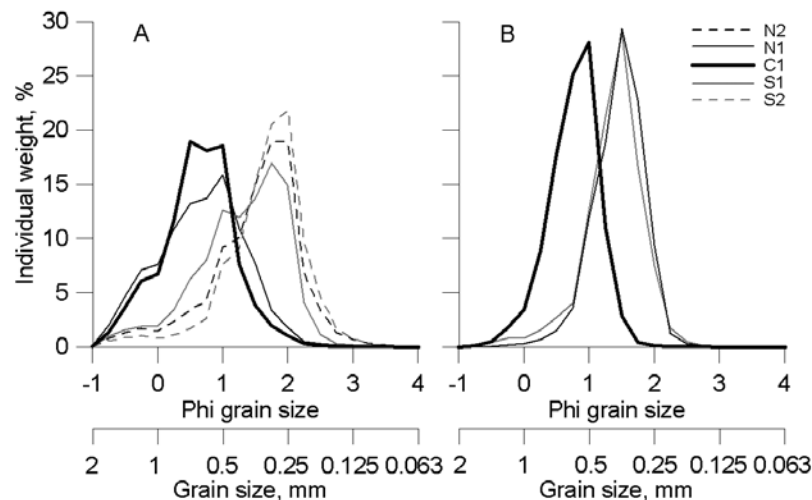


**Figure 7.** Frequency curves of the grain size distributions along the crests of dunes (a) 4 and (b) 12 at the intersections with transects N2-S2 (for locations, see Figure 2).

grain size decreases from 0.629 mm in the center of the channel to 0.357 mm and 0.362 mm at the northern and southern side of the channel, respectively (Figure 6a and Table 1). In addition, there is a decrease in mean grain size along the channel from northeast to southwest (Figure 6a). The phi standard deviation, i.e., sorting, of the grain populations across the channel is relatively uniform (Figures 7a and 7b and Table 1), whereas it decreases along the channel from northeast to southwest (Figures 6b, 7a, and 7b), i.e., changing from moderately well sorted to well sorted [after Folk, 1974]. The phi skewness, i.e., sorting in the tails of the grain population, varies from near symmetrical to negative (coarse) skewed [after Folk, 1974], showing signs of increasing negative skewness from the center toward the sides of the channel (Figure 6c and Table 1). The phi kurtosis, i.e., degree of sharpness or peakedness, of the grain size distributions is relatively uniform both across and along the channel (Figure 6d and Table 1).

## 5. Dune Dynamics

### 5.1. Development of Barchanoid-Shaped Dunes

[27] The observed dune migration in the survey area reveals an increase in dune celerity from the center toward the sides of the channel (Table 1). This inevitably results in the development of barchanoid-shaped dunes as also observed in the dune field (see Figure 2). Furthermore, a decrease in dune height (size) was observed from the center toward the sides of the channel (Table 1). This suggests that the increase in dune celerity from the center toward the sides of the channel is a result of the decrease in dune height (size) away from the center of the channel. This can be explained by the fact that a smaller volume of sediment has to be moved at the sides per unit time for equal dune celerity. Plotting dune celerity against dune height (Figure 8) confirms this yielding significant logarithmic relationships when using both single values for individual dunes ( $r = 0.560$ ,  $n = 49$ ,  $p < 0.0005$ ) as well as average values for transects N2-S2 as given in Table 1 ( $r = 0.813$ ,  $n = 5$ ,  $p < 0.05$ ). The regression line of the logarithmic relationship when using single values for individual dunes is shown in

Figure 8, i.e.,  $c = -14.83 \ln H + 26.68$  with  $H$  in m and  $c$  in m/yr.

### 5.2. Factors Controlling Dune Size

[28] The scaling factors controlling the size of dunes have been argued to be grain size- and flow velocity-dependent, along with water depth as a limiting factor assuming an abundance of sediment [Flemming, 2000a]. The dunes in the Grådyb tidal inlet channel are not starved and there is a general abundance of sediment in the area [Bartholdy *et al.*, 2002]. The water depth across the channel is nearly uniform, as illustrated by the observed average water depths in transects N2-S2 (Table 1). In addition, the standard deviation of the water depths along the part of cross section NE bounded by transects N2 and S2, i.e., 0.62 m is low. The flow velocity across the channel during both ebb and flood is also practically uniform. This is demonstrated by the low standard deviations of the cross-section mean flow velocities in the part of cross section NE bounded by transect N2 and S2, i.e., 0.05–0.12 m/s, based on the 10-hour measurements during a tidal period. This implies that the decrease in dune height from the center toward the sides of the channel (Table 1) is a result of the decrease in mean grain size away

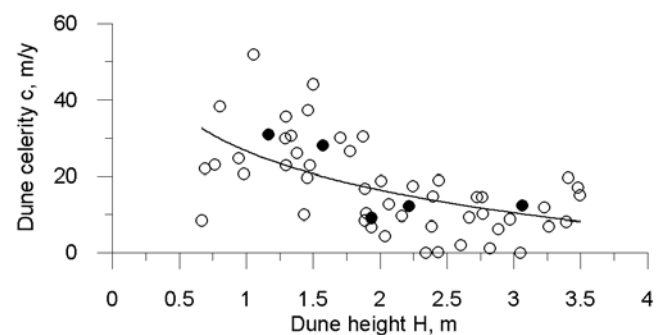


**Figure 8.** Scatter diagram of dune celerity  $c$  against dune height  $H$ . Circles refer to the individual dunes, whereas the dots refer to the average values in transects N2-S2 (for locations, see Figure 2) as given in Table 1.

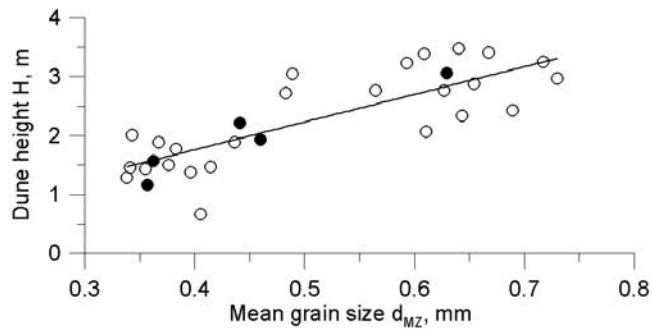


**Figure 9.** Scatter diagram of dune height  $H$  against mean grain size  $d_{MZ}$  at the dune crests of the large to very large compound dunes (for locations, see Figure 2). Circles refer to the individual dunes, whereas the dots refer to the average values in transects N2-S2 (for locations, see Figure 2) as given in Table 1.

from the center of the channel (Table 1). This is confirmed by plotting dune height against mean grain size (Figure 9) which yields significant linear relationships, both when using single values for individual dunes ( $r = 0.798$ ,  $n = 25$ ,  $p < 0.0005$ ) and when using average values for transects N2-S2 as given in Table 1 ( $r = 0.958$ ,  $n = 5$ ,  $p < 0.01$ ). The regression line of the linear relationship when using single values for individual dunes is shown in Figure 9, i.e.,  $H = 4.70d_{MZ} - 0.12$  with  $d_{MZ}$  in mm and  $H$  in m.

### 5.3. Factors Controlling Grain Size Variability

[29] The bathymetric data reveal asymmetric small to large dunes located in the trough/lee side region of the large to very large dunes, indicating the existence of secondary sediment transport paths as a result of secondary currents directed from the center toward the sides of the channel (Figure 10).

[30] According to McLaren [1981] and McLaren and Bowles [1985], sediment in transport will decrease in mean grain size, i.e., become finer, decrease (or not increase) in standard deviation, i.e., become better sorted, and become more negatively skewed, i.e., coarse tailed, in the direction of transport. In the ebb-dominated Grådyb tidal inlet channel this model applies well with mean grain size and standard deviation decreasing in the direction of ebb flow as well as the distributions being primarily negatively skewed (Figures 6 and 7). Laterally from the center toward the sides of the channel there is also a decrease in mean grain size, a constant or decreasing standard deviation and a primarily increasing negative skewness (Figures 6 and 7 and Table 1). Applying the McLaren model laterally moreover supports the existence of secondary currents resulting in a secondary sediment transport directed from the center toward the sides of the channel.

[31] As already mentioned, medium to coarse sand is supplied to the system from the Pleistocene cliffs lining the mainland in the landward part of the back-barrier tidal basin (see Figure 1), whereas fine sand is brought in from the nearshore region of the open coast [Bartholdy et al., 2002]. This setup provides the components needed for the lateral grain size pattern observed in the Grådyb tidal inlet channel. The Pleistocene cliff sand may be transported seaward in

bed load by the dominating ebb flow [Bartholdy et al., 2002] resulting in a fining, better sorting, and negatively skewing of the grain population. In addition the finer fractions of the Pleistocene cliff sand may be transported laterally in bed load or intermittent suspension from the center toward the sides of the channel by the suggested secondary currents. The nearshore fine sand introduced to the system by each flood may undergo a similar transport mechanism.

### 5.4. Dune Splitting

[32] The average dune dimensions in the center of the channel follow the height-length relationship suggested by Flemming [1988] (Figure 11). However, this is not the case closer to the channel sides where the dunes get lower and longer (Table 1). The dune dimensions along the most southwesterly 100 m section along transects N2 and S2, where the large to very large compound dunes were indiscernible, again follow the relationship suggested by Flemming [1988] (Figure 11). This implies that the large to very large dunes at the sides of the channel are adjusting to the decrease in mean grain size by splitting up into smaller dunes.

## 6. Bed Load Transport

[33] Average volumetric bed load transport along transects N2-S2, calculated by insertion of measured dune

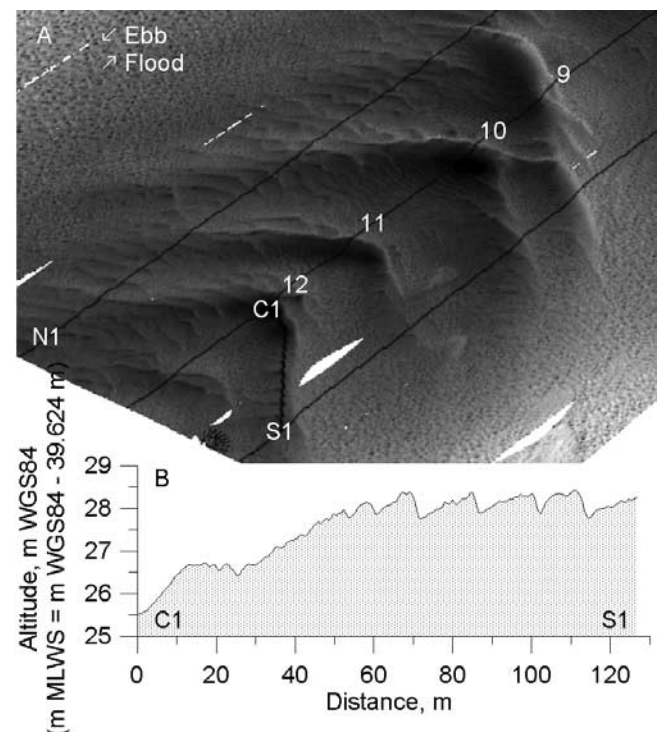


**Figure 10.** (a) Bathymetry of the southwestern part of the Grådyb tidal inlet channel in 2002 (for location, see Figure 2). (b) Bed profile in the trough/lee side region parallel to the crest of dune 12 from the center (C1) toward the southern side (S1) of the channel. The bed profile has been extracted from a bathymetric grid with a cell size of  $0.5 \times 0.5$  m.

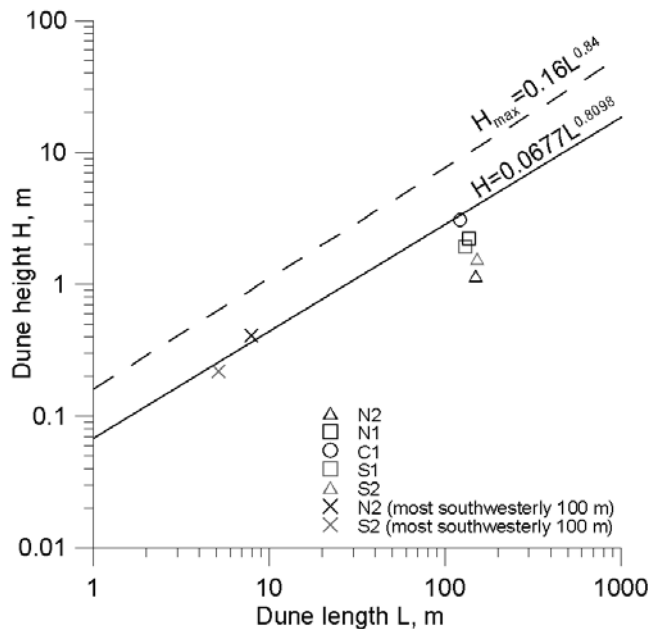


**Figure 11.** Average dune height  $H$  against average dune length  $L$  in transects N2-S2 (for locations, see Figure 2). The solid and shaded crosses refer to the most southwesterly 100 m sections along transects N2 and S2 (for locations, see Figure 2). Solid and dashed lines show the global and upper height limit relationship, respectively, according to *Flemming* [1988].

dimensions and celerities in equation (1), are shown in Table 2. In the center and along the sides of the channel, the bed load transport is practically equal with an average value of  $16 \text{ m}^2/\text{yr}$ , whereas along transect N1 and S1 it only amounts to 50% of this value with an average around  $8 \text{ m}^2/\text{yr}$  (Table 2).

[34] As shown above, water depth as well as flow velocity during both ebb and flood are practically uniform. Bedload transport was predicted along transects N2-S2 at discrete time steps by insertion and substitution in equations (2)–(11) using the cross-section mean flow velocities and water depths shown in Figure 5 together with the grain size values given in Table 1. Integrating over the tidal period and calculating the difference by subtraction yields the net bed load transport as well as the transport direction. In Figure 12

**Table 2.** Volumetric Bed Load Transport  $q_b$  Along Transects N2-S2 Calculated by Insertion of Measured Dune Dimensions and Celerities in Equation (1) as Well as Predicted From the Bed Load Transport Formulae in Equations (2)–(5)<sup>a</sup>

Bedload Transport Formula	Equation	$q_b, \text{ m}^2/\text{yr}$				
		N2	N1	C1	S1	S2
Measured						
<i>Simons et al.</i> [1965]	(1)	17	9	15	6	15
Predicted						
<i>Meyer-Peter and Müller</i> [1948]	(2)	77	75	79	76	74
<i>Engelund and Fredsøe</i> [1976]	(3)	126	143	162	146	127
<i>Van Rijn</i> [1984a]	(4)	106	110	118	113	101
<i>Nielsen</i> [1992]	(5)	126	132	143	134	126

<sup>a</sup>For locations, see Figure 2.

the prediction of bed load transport along transect C1 using the classical formula of *Meyer-Peter and Müller* [1948] (equation (2)) is shown as an example of this procedure. In addition, the net ebb-directed bed load transport (Figure 12b) documents the ebb dominance, i.e., the asymmetry and migration direction of the dunes in the Grådyb tidal inlet channel are the result of the higher flow velocities during the ebb (Figure 5).

[35] Assuming that the tidal period at spring tide on the 3rd of July 2004 is representative of an entire year, the predicted bed load transport over the tidal period was extrapolated to a yearly budget using a tidal period duration of 12 hours and 25 min. Predicted volumetric bed load transport along transects N2-S2 ranges from  $75 \text{ m}^2/\text{yr}$  to  $162 \text{ m}^2/\text{yr}$  according to the various bed load transport formulae (Table 2). The *Meyer-Peter and Müller* [1948] formula predicts a practically uniform bed load transport across the channel ranging from  $74 \text{ m}^2/\text{yr}$  to  $79 \text{ m}^2/\text{yr}$  (Table 2). By contrast, the formulae of *Engelund and Fredsøe* [1976], *Van Rijn* [1984a], and *Nielsen* [1992] predict an increase in bed load transport from the center toward the sides of the channel (Table 2). Furthermore, all bed load transport prediction formulae overestimate the bed load transport calculated by insertion of measured dune dimensions and celerities in equation (1) (Table 2), the overestimates ranging from a factor 4 in the best case to 24 in the worst case.

### 7. Discussion

[36] The development of barchanoid-shaped dunes in the Grådyb tidal inlet channel has been shown to be the result of higher dune celerities along the sides of the channel due to smaller dunes along the sides. A similar conclusion of an increase in dune celerity as a result of a decrease in dune height (size) and hence smaller sediment volumes that have

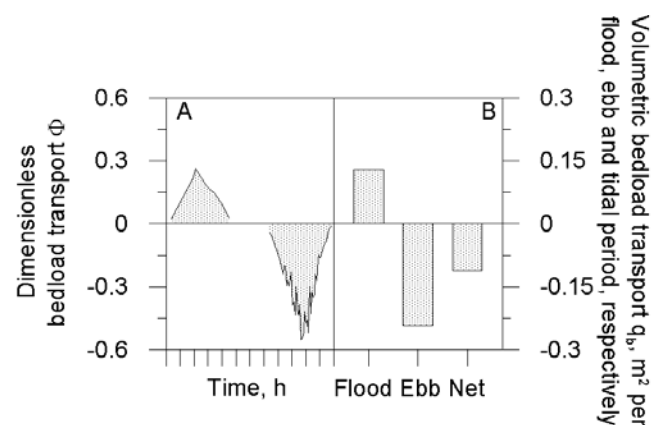


**Figure 12.** Example schematizing the prediction of net volumetric bed load transport over a tidal period. (a) Dimensionless bed load transport  $\Phi$  along transect C1 (for location, see Figure 2) at discrete time steps according to *Meyer-Peter and Müller* [1948] (equation (2)) during a tidal period around spring tide. (b) The corresponding volumetric bed load transport during flood and ebb along with the resulting net bed load transport over the tidal period.

to be moved was also reached by, for example, *Dinehart* [2002].

[37] The decrease in dune height here being a function of the decrease in mean grain size is in conflict with the classical concept of factors controlling dune size. Commonly, dune height is considered to scale with water depth [*Yalin*, 1977; *Van Rijn*, 1984b]. This is not the case in the Grådyb tidal inlet channel where the decrease in dune height from the center toward the sides of the channel occurs at practically uniform water depths. The formulae predicting dune height to scale with water depth such as those of *Yalin* [1977] and *Van Rijn* [1984b] are primarily based on data derived from flume studies where water depths are typically small compared to those in natural systems. This introduces an artificial dependency because the water depth is an upper boundary acting as a limit for dune growth. *Carling et al.* [2000] observed this mechanism in the River Rhine where a water depth limitation on dune heights was seen at shallow water depths. However, in natural systems where water depths are generally much larger than dune height no dependency of water depth on dune height is observed [*Kuijpers et al.*, 2002].

[38] Dunes varying in height have been observed side by side in situations where the flow is characterized by lateral flow velocity gradients [*Flemming*, 2000b]. In the Grådyb tidal inlet channel, mean flow velocity is laterally uniform both during ebb and flood making this argument inapplicable in this environment.

[39] However, a decrease in dune height due to a decrease in mean grain size is in accordance with *Flemming* [2000a], who theoretically shows that the larger the grain size, the larger the maximum potential dune size. *Flemming* [2000a] argues that dune growth will terminate once flow acceleration above the dune crest reaches a grain size-dependent critical suspension velocity. This relation is confirmed by the observations in the Grådyb tidal inlet channel where dune height decreases with decreasing mean grain size. Though, near-bed flow velocity measurements at the crests of the dunes are required to confirm whether the suspension of bed material is the reason for the termination of dune growth.

[40] It has been shown that the relationship between dune height and mean grain size in the Grådyb tidal inlet channel is significantly positively correlated and can be described by a linear relationship. Earlier, *Bartholdy et al.* [2002] likewise established a significant positively correlated relationship, but expressed by a power function based on two separate bed sample sets taken with a Van-Veen grab from the same study area in 1992 and 1999. The power function was derived from randomly positioned samples with mean grain sizes ranging from 0.33 mm to 0.56 mm, whereas the linear function established in this study is based solely on crest samples with mean grain sizes covering the range from 0.33 mm to 0.73 mm. The importance of sampling position may be exemplified by additional bed samples collected from the troughs and backs of 3 dunes in transect C1. These samples revealed an average mean grain size in the troughs, on the backs and on the crests of 0.488 mm, 0.523 mm and 0.629 mm, respectively, which illustrates the importance of comparable sampling positions when analyzing the data. The shift in the descriptive relationship, from a power function to a linear function, can be explained by the

inaccuracy in sampling positioning during earlier surveys since *Bartholdy et al.* [2002] most likely underestimated the related mean grain size due to the low probability of a randomly positioned sample to be located at the dune crest. The physical explanation of why the relationship is linear is currently unknown to the authors.

[41] Concerning cross-channel distributions in grain size no earlier studies have been found. The observations from the Grådyb tidal inlet channel showing a lateral variability in grain sizes along the dune crests is, to the knowledge of the authors, the first time that such patterns have been documented.

[42] Recently, however, *Maddux et al.* [2003a, 2003b] conducted a series of detailed measurements of unidirectional turbulent open channel flow over fixed, artificial, sinuous-crested three-dimensional (3-D) dunes in a laboratory flume. They found that the flow was topographically steered by the 3-D features and that the largest measured cross-stream flow velocities were in the troughs with most of the cross-stream flow occurring close to the bed. Although the flume experiments were carried out in clear water without moveable bed material, they nevertheless show the existence of secondary currents in the troughs of barchanoid-shaped dunes and thereby support the suggestion of the existence of secondary transport paths in the troughs.

[43] Dune splitting as an adjustment process to changing conditions has earlier been observed in the course of the flow velocity reduction from spring to neap tide where larger dunes split up into smaller ones with the larger spring-tide dunes still being discernible at neap tide [*Flemming and Davis*, 1992]. Likewise the large to very large dunes along the sides of the Grådyb tidal inlet channel are adjusting by splitting up into smaller dunes, however, in this case due to a decrease in mean grain size.

[44] Concerning the discrepancy between measured and predicted bed load transport, part of the overestimation is certainly due to the fact that the tidal period around spring tide on 3 July 2004 is unrepresentative of the general dynamics in the Grådyb tidal inlet channel, seeing that the predicted bed load transport around spring tide undoubtedly exceeds the corresponding transport around neap tide considerably. An additional reason for the overestimation is probably that transport processes in nature are not always well described by the currently available bed load transport prediction formulae, which have all been calibrated on the basis of flume studies. *Soulsby* [1997] earlier emphasized the fact of transport formulae being based on incorrect assumptions and found discrepancies up to a factor of four when using various published equations. He further argues that although bed load transport responds quickly to changes in, e.g., flow velocity and water depth, and hence justifying an approach based on quasi-equilibrium transport, a calculation based on dune dimensions and celerities is recommended, especially in unsteady flows as found in tidal environments. The lateral distribution of bed load transport with lower values between the center and along the sides of the channel may be an effect of the suggested secondary currents and related transport from the center toward the sides of the channel. Nonetheless, a higher measuring frequency with better resolved near bed dynamics is needed to shed more light on these processes occurring oblique to

the main current and at a lower order of magnitude in flow velocities.

## 8. Conclusions

[45] On the basis of the analysis of bathymetry, flow velocity and grain size in a dune field section of the Grådyb tidal inlet channel in the Danish Wadden Sea, the following conclusions are reached.

[46] 1. Dune migration is net ebb-directed and increases from the center toward the sides of the channel resulting in the development of barchanoid-shaped dunes.

[47] 2. The increase in dune celerity is a result of the corresponding decrease in dune height (size) from the center toward the sides of the channel, because smaller volumes of sediment have to be moved at the sides per unit time for equal dune celerity.

[48] 3. The decrease in dune height is due to an equivalent decrease in grain size from the center toward the sides of the channel, in view of the fact that water depth and flow velocity during both ebb and flood are practically uniform across the channel. The grain size control on dune height may be due to the fact that flow velocities at the dune crests reach the suspension criteria of the bed material which then terminates further dune growth as theoretically proposed by *Flemming* [2000a]; but near-bed flow velocity measurements at the crests of the dunes are required to test this hypothesis.

[49] 4. The decrease in grain size is suggested to be the sorting effect of secondary currents in the trough/lee side region directed from the center toward the sides of the channel, supporting the transport of the finer sediment fractions.

[50] 5. The more rapidly migrating flanks of the barchanoid-shaped dunes seems to be an adjustment to the decrease in grain size from the center toward the sides of the channel, causing the dunes to split up into smaller forms.

[51] 6. The net ebb-directed bed load transport, calculated from dune dimensions and celerities, is lower between the center and along the sides of the channel. This lateral distribution of bed load transport is unresolved by the classical *Meyer-Peter and Müller* [1948] and the widely applied formulae of *Engelund and Fredsøe* [1976], *Van Rijn* [1984a] and *Nielsen* [1992]. In addition, these bed load transport formulae over-predict the bed load transport as calculated from dune dimensions and celerities.

## Notation

$c$	bed form celerity, m/yr.
$C'$	grain related Chézy roughness coefficient, $m^{0.5}/s$ .
$d_{MZ}$	mean grain size, m (or mm).
$d_{50}$	median grain size, m (or mm).
$d_{90}$	coarse 90th percentile of the grain size distribution, m (or mm).
$D$	water depth, m
$D_*$	particle parameter
$g$	acceleration due to gravity, $m/s^2$ .
$H$	bed form height, m.
$k'_s$	grain roughness, m.
$K_G$	phi kurtosis.

$L$	bed form length, m.
$q_b$	volumetric bed load transport, $m^2/yr$ .
$s$	relative sediment density
$Sk_I$	phi skewness.
$T$	excess bed shear stress parameter.
$u'_f$	friction velocity, m/s.
$U$	mean flow velocity (depth averaged), m/s.
$V$	bed form volume per unit width, $m^2$ .
$\beta$	shape factor.
$\theta'$	grain-related Shield's parameter.
$\theta_{cr}$	threshold Shield's parameter.
$\rho$	water density, $kg/m^3$ .
$\rho_s$	sediment density, $kg/m^3$ .
$\sigma_I$	phi standard deviation.
$\nu$	kinematic viscosity, $m^2/s$ .
$\Phi_b$	dimensionless bed load transport.

[52] **Acknowledgments.** This study was supported by the German Science Foundation. The captain and crew of the RV *Senckenberg* are thanked for their expertise and unfailing good spirits during the cruises. Also appreciated is the field assistance of Elke Tilch and Anders Bartholdy. Nicol Mahnken-Roetzer, Sonja Heinrich, and Wolfgang Nenno are thanked for assisting in the laboratory. Finally, the quality of the manuscript improved from valuable comments and suggestions by two anonymous reviewers, the Associate Editor, and the Editor, who are all thanked for their thorough and engaged reviews.

## References

- Allen, J. R. L. (1982), *Sediment Structures: Their Character and Physical Basis*, vol. 1, *Dev. Sedimentol. Ser.*, vol. 30, 593 pp., Elsevier, New York.
- Abraham, D., and T. Pratt (2002), Quantification of bed-load transport on the upper Mississippi River using multibeam survey data and traditional methods, *Rep. ERDC/CHL CHETN-VII-4*, U.S. Army Eng. Res. and Dev. Cent., Vicksburg, Miss. (<http://chl.wes.army.mil/library/publications/chetn>)
- Arduhin, F., T. G. Drake, and T. H. C. Herbers (2002), Observations of wave-generated vortex ripples on the North Carolina continental shelf, *J. Geophys. Res.*, 107(C10), 3143, doi:10.1029/2001JC000986.
- Ashley, G. M. (1990), Classification of large-scale subaqueous bedforms: A new look at an old problem, *J. Sediment. Petrol.*, 60(1), 160–172.
- Bartholdy, J., and D. Anthony (1998), Tidal dynamics and seasonal dependent import and export of fine-grained sediment through a backbarrier tidal channel of the Danish Wadden Sea, in *Tidalities: Processes and Products*, edited by C. Alexander, R. A. Davis, and V. J. Henry, *SEPM Spec. Publ.*, 61, 43–52.
- Bartholdy, J., A. Bartholomae, and B. W. Flemming (2002), Grain-size control of large compound flow-transverse bedforms in a tidal inlet of the Danish Wadden Sea, *Mar. Geol.*, 188, 391–413.
- Carling, P. A., E. Gözl, H. G. Orr, and A. Radecki-Pawlik (2000), The morphodynamics of fluvial sand dunes in the River Rhine, near Mainz, Germany, I. Sedimentology and morphology, *Sedimentology*, 47, 227–252.
- Dalrymple, R. W., R. J. Knight, and J. J. Lambiase (1978), Bedforms and their hydraulic stability relationships in a tidal environment, Bay of Fundy, Canada, *Nature*, 275, 100–104.
- Dinehart, R. L. (2002), Bedform movement recorded by sequential single-beam surveys in tidal rivers, *J. Hydrol.*, 258, 25–39.
- Engel, P., and Y. L. Lau (1980), Computation of bedload using bathymetric data, *J. Hydraul. Div. Am. Soc. Civ. Eng.*, 106, 369–380.
- Engel, P., and Y. L. Lau (1981), Bed load discharge coefficient, *J. Hydraul. Div. Am. Soc. Civ. Eng.*, 107, 1445–1454.
- Engelund, F., and J. Fredsøe (1976), A sediment transport model for straight alluvial channels, *Nord. Hydrol.*, 7, 293–306.
- Flemming, B. W. (1978), Underwater sand dunes along the southeast African continental margin—Observations and implications, *Mar. Geol.*, 26, 177–198.
- Flemming, B. W. (1988), Zur Klassifikation subaquatischer, strömungs-transversaler Transportkörper, *Bochumer Geol. Geotechn. Arb.*, 29, 44–47.
- Flemming, B. W. (2000a), The role of grain size, water depth and flow velocity as scaling factors controlling the size of subaqueous dunes, in *Marine Sandwave Dynamics, Proceedings of an International Workshop Held in Lille, France, 23 and 24 March 2000*, edited by A. Trentesaux and T. Garlan, pp. 55–60, Univ. of Lille 1, Lille, France.

- Flemming, B. W. (2000b), On the dimensional adjustment of subaqueous dunes in response to changing flow conditions: A conceptual process model, in *Marine Sandwave Dynamics, Proceedings of an International Workshop Held in Lille, France, 23 and 24 March 2000*, edited by A. Trentesaux and T. Garlan, pp. 61–67, Univ. of Lille 1, Lille, France.
- Flemming, B. W., and R. A. Davis Jr. (1992), Dimensional adjustment of subaqueous dunes in the course of a spring-neap semicycle in a mesotidal backbarrier channel environment (German Wadden Sea, southern North Sea), in *Tidal Clastics 92, Courier Forschungsinst. Senckenberg*, vol. 151, edited by B. W. Flemming, pp. 28–30, Senckenbergische Naturforschende Ges., Frankfurt am Main, Germany.
- Folk, R. L. (1974), *Petrology of Sedimentary Rocks*, 182 pp., Hemphill, Austin, Tex.
- Folk, R. L., and W. C. Ward (1957), Brazos river bar: A study in the significance of grain size parameters, *J. Sediment. Petrol.*, 27(1), 3–26.
- Fredsoe, J., and R. Deigaard (1992), *Mechanics of Coastal Sediment Transport, Adv. Ser. Ocean Eng.*, vol. 3, 369 pp., World Sci., Hackensack, N. J.
- Harbor, D. J. (1998), Dynamics of bedforms in the lower Mississippi River, *J. Sediment. Res.*, 68(5), 750–762.
- Hennings, I., D. Herbers, K. Prinz, and F. Ziemer (2004), On waterpouts related to marine sandwaves, in *Marine Sandwave and River Dune Dynamics II, International Workshop, April 1-2 2004, University of Twente, The Netherlands, Proceedings*, edited by S. Hulscher, T. Garlan, and D. Idier, pp. 88–95, University of Twente, Enschede, Netherlands.
- Hoekstra, P., P. Bell, P. van Santen, N. Roode, F. Levoy, and R. Whitehouse (2004), Bedform migration and bedload transport on an intertidal shoal, *Cont. Shelf Res.*, 24, 1249–1269.
- Kostaschuk, R., and P. Villard (1996), Flow and sediment transport over large subaqueous dunes: Fraser River, Canada, *Sedimentology*, 43, 849–863.
- Kostaschuk, R., M. A. Church, and J. L. Luternauer (1989), Bed-material, bedforms and bed load in a salt-wedge estuary—Fraser River, British Columbia, *Can. J. Earth Sci.*, 26, 1440–1452.
- Kuijpers, A., B. Hansen, V. Hühnerbach, B. Larsen, T. Nielsen, and F. Werner (2002), Norwegian Sea overflow through the Faroe Shetland gateway as documented by bedforms, *Mar. Geol.*, 188, 147–164.
- Lutz, P., and R. Gounon (2001), THALES Navigation's LRK<sup>®</sup>, an improved RTK solution for long baselines: Technique, applications and field results, paper presented at the 14th International Technical Meeting, Satell. Div., Inst. of Navig., Salt Lake City, Utah.
- Maddux, T. B., J. M. Nelson, and S. R. McLaren (2003a), Turbulent flow over three-dimensional dunes: 1. Free surface and flow response, *J. Geophys. Res.*, 108(F1), 6009, doi:10.1029/2003JF000017.
- Maddux, T. B., J. M. Nelson, and S. R. McLaren (2003b), Turbulent flow over three-dimensional dunes: 2. Fluid and bed stresses, *J. Geophys. Res.*, 108(F1), 6010, doi:10.1029/2003JF000018.
- McLaren, P. (1981), An interpretation of trends in grain size measures, *J. Sediment. Petrol.*, 51(2), 611–624.
- McLaren, P., and D. Bowles (1985), The effects of sediment transport on grain-size distributions, *J. Sediment. Petrol.*, 55(4), 457–470.
- Meyer-Peter, E., and R. Müller (1948), Formulas for bed-load transport, paper presented at 2nd Meeting of the International Association for Hydraulic Structures Research, Stockholm.
- Nielsen, P. (Ed.) (1992), *Coastal Bottom Boundary Layers and Sediment Transport, Adv. Ser. Ocean Eng.*, vol. 3, 352 pp., World Sci., Hackensack, N. J.
- Simons, D. B., E. V. Richardson, and C. F. Nordin Jr. (1965), Bedload equation for ripples and dunes, *U.S. Geol. Surv. Prof. Pap.*, 462-H, 9 pp.
- Soulsby, R. (1997), *Dynamics of Marine Sands: A Manual for Practical Applications*, 249 pp., Thomas Telford, London.
- Soulsby, R., and R. J. S. W. Whitehouse (1997), Threshold of sediment motion in coastal environments, paper presented at Pacific Coasts and Ports '97 Conference, Univ. of Canterbury, Christchurch, New Zealand.
- Sukhodolov, A., M. Thiele, and H. Bungartz (1998), Turbulence structure in a river reach with sand bed, *Water Resour. Res.*, 34(5), 1317–1334.
- Van den Berg, J. H. (1987), Bedform migration and bed-load transport in some rivers and tidal environments, *Sedimentology*, 34, 681–698.
- Van Rijn, L. C. (1984a), Sediment transport, part I: Bed load transport, *J. Hydraul. Eng.*, 110(10), 1431–1456.
- Van Rijn, L. C. (1984b), Sediment transport, part III: Bed forms and alluvial roughness, *J. Hydraulic Eng.*, 110(12), 1733–1754.
- Van Rijn, L. C. (1993), *Principles of Sediment Transport in Rivers, Estuaries and Coastal Seas*, Aqua, Amsterdam.
- Villard, P. V., and M. Church (2003), Dunes and associated sand transport in a tidally influenced sand-bed channel: Fraser River, British Columbia, *Can. J. Earth Sci.*, 40, 115–130.
- Wilbers, A. W. E., and W. B. M. Ten Brinke (2003), The response of subaqueous dunes to floods in sand and gravel bed reaches of the Dutch Rhine, *Sedimentology*, 50, 1013–1034.
- Yalin, M. S. (1977), *Mechanics of Sediment Transport*, 298 pp., Elsevier, New York.

J. Bartholdy, Institute of Geography, University of Copenhagen, Øster Voldgade 10, DK-1350 Copenhagen, Denmark. (jb@geogr.ku.dk)

A. Bartholomä and B. W. Flemming, Division of Marine Science, Senckenberg Institute, Suedstrand 40, D-26382 Wilhelmshaven, Germany. (abartholomae@senckenberg.de; bflemming@senckenberg.de)

V. B. Ernstsen, D. Hebbeln, R. Noormets, and C. Winter, Research Center Ocean Margins, University of Bremen, P.O. Box 33 04 40, D-28334 Bremen, Germany. (ernstsen@uni-bremen.de; hebbeln@uni-bremen.de; riko@uni-bremen.de; acwinter@uni-bremen.de)